Heat transfer and entropy generation optimization of forced convection in a porous-saturated duct of rectangular cross-section

K. Hooman[1], H. Gurgenci[1], and A. A. Merrikh[2]

[1]School of Engineering, The University of Queensland, Brisbane, QLD4072, Australia

[2] Applied Thermal Technologies LLC, 2700 Via Fortuna Dr., Suit 301, Austin, TX 78746

Abstract

We investigate analytically the First and the Second Law (of Thermodynamics) characteristics of fully developed forced convection inside a porous-saturated duct of rectangular cross-section. The Darcy-Brinkman flow model is employed. Three different types of thermal boundary conditions are examined. Expressions are presented for the Nusselt number, the Bejan number, and the dimensionless entropy generation rate in terms of the system parameters. The conclusion of this analytical study will make it possible to compare and evaluate alternative rectangular duct design options in terms of heat transfer, pressure drop, and entropy generation.

Keywords: Entropy generation, porous media, forced convection, rectangular duct.

Nomenclature

a	channel width to height ratio
A	parameter defined by Eq. (2-b)
A_1,A_2	constants
Be	Bejan number
Br	Darcy-Brinkman number $\frac{\mu U^2 H}{q'' K}$
Br*	modified Brinkman number $\frac{\mu U^2}{k T_w q^{*2}}$
c_P	specific heat at constant pressure, $[J/kg \cdot K]$
Da	Darcy number K/H^2
D_H	hydraulic diameter 4Ha/(a+1) [m]
D_n	coefficient defined by Eq. (2-c)
FFI	fluid friction irreversibility per unit volume $[W/m^3K]$
F_n	coefficients defined by Eq.(25)
G	negative of the applied pressure gradient [Pa/m]
H	half channel width [m]
HTI	heat transfer irreversibility per unit volume $[W/m^3K]$
k	porous medium thermal conductivity $[W/m^2 \cdot K]$
K	permeability $[m^2]$
K_n	coefficients defined by Eq. (19)
m	parameter $(s^2 + \lambda_n^2)^{1/2}$
M	viscosity ratio

Ns dimensionless entropy generation Eq. (9)

Ns^* cross-sectional average of Ns

Nu Nusselt number defined by Eqns (5-a,b)

Nu_i Nusselt number for the boundary condition case i (i =1, 2, 3)

P_h heated perimeter of the duct [m]

Pe the Péclet number $Pe = \rho c_p U D_H / k$

q' wall heat transfer rate per unit length of the duct [W/m]

q'' heat transfer rate per unit heat transfer area of the duct Eq. (5-b) [W/m^2]

q^* dimensionless heat flux, Eq.(10)

S porous media shape parameter $s = (MDa)^{-1/2}$

$\dot{S}_{gen}$ Entropy generation rate per unit volume [W/m^{3}K]

T^* local absolute temperature [K]

T_m bulk temperature [K]

T_w wall temperature [K]

u^* x-velocity [m/s]

$\hat{u}$ dimensionless velocity Eq.(2-a)

U average velocity [m/s]

x^* longitudinal coordinate [m]

x dimensionless coordinate, (x*/H)/Pe

y^*, z^* coordinates [m]

y,z $(y^*,z^*)/H$

Greek symbols

θ dimensionless temperature

θ_b dimensionless bulk temperature

λ_n eigenvalues

μ fluid viscosity [$N \cdot s/m^2$]

$\tilde{\mu}$ effective viscosity [$N \cdot s/m^2$]

ρ fluid density [kg/m^3]

ϕ dimensionless viscous dissipation function

1. INTRODUCTION

There has been renewed interest recently in the problem of forced convection in porous media. An increasingly important application is in cooling electronics, with coolants such as poly-alpha-olefin flowing through a porous metal matrix. Narasimhan and Lage [1] offers an analysis of forced convection through an aluminum based porous matrix heated from top and bottom to model the heat generated by the electronic circuits in radar equipment. Commensurate with the generic importance of the area, a substantial amount of literature on this topic is already available as reported in Nield and Bejan [2] and Cheng [3]. Circular tubes or semi-infinite parallel plates channel are the most widely used geometries in fluid flow and heat transfer devices for both clear fluid or porous media such as water distribution systems, heat exchangers, and similar applications. Fluid flow and heat transfer characteristics of such problems have been analyzed in detail for various boundary conditions. For circular tubes or parallel plates, the simplicity of the geometry allows analytical solutions of closed form. Thus the question naturally arises as to whether analytical solutions for more complicated cross-sections are possible.

The method of weighted residuals was exploited by Haji-Sheikh and Vafai [4] in their study of thermally developing convection in ducts of various shapes. In a subsequent study, Haji-Sheikh [5] has applied a Fourier series method to investigate fully developed forced convection in a duct of rectangular cross section. Haji-Sheikh et al. [6-10] have investigated heat transfer through porous ducts of arbitrary cross-sections. Their focus was to find heat transfer characteristics of the thermal entrance region.

Applying a Fourier series method, Hooman and Merrikh [11] have analytically investigated heat and fluid flow in a rectangular duct occupied by a hyperporous medium. In ducts of

arbitrary cross section, Hooman [12-14] has reported closed form solutions for the fully developed temperature distribution and the Nusselt number as well as the local entropy generation rate by applying the Darcy momentum equation.

The groundbreaking work by Bejan [15] introduced the concept of entropy generation analysis due to fluid flow and heat transfer as a powerful tool to evaluate the effectiveness of different configurations. Since entropy generation destroys the work availability of a system, it makes good engineering sense to focus on irreversibility of heat transfer and fluid flow processes to understand the associated entropy generation mechanisms. The literature on the topic is rich for clear fluids through unobstructed ducts (a recent survey of literature on the topic can be found in [16-17]). However, modeling entropy generation in porous media is comparatively more problematic since modeling viscous dissipation, and consequently the fluid friction irreversibility, in a non-Darcy porous medium is a controversial issue. For the Darcy flow model the viscous dissipation is modeled by a velocity square term only (see for example Baytas [18-19] or Hooman [12-14]) but when the boundary and inertia effects are to be considered there are three alternatives for viscous dissipation term. Nield [20] argued that the viscous dissipation function should remain equal to the power of the drag force when the Brinkman equation is considered. On the other hand, Al-Hadrami et al. [21] have proposed a clear flow compatible model. Nield et al. [22] have combined the three alternatives to a single equation treating both the isothermal and isoflux boundary conditions. A similar attempt was made by Hooman et al. [23-24] for a developing flow. Nield [25] has commented on the alternative models applied so far. He emphasized that one should not use just the term involving velocity derivatives. In the light of Nield [25], Hooman and Ejlali [26] and Hooman et al. [27] have questioned some of the articles

that neglected the Darcy dissipation term. One observes that further work on modeling entropy generation in a porous medium is called for.

Considering the two problems concurrently, the energy-entropy analysis for ducts of arbitrary cross section was carried out by applying the Darcy flow model in [12-14]. However, when non-Darcy effects are considered, the velocity distribution has no longer a uniform (slug) shape and the situation gets more complicated. Applying the velocity distribution reported in [11], this paper offers an analytical solution of heat transfer and entropy generation in a duct of rectangular cross section saturated by a porous medium. In the terminology of Shah and London [28], three cases of **H1** boundary condition are applied, to be referred to as cases 1, 2, and 3 as described in figure 1 and table 1). For **H1** boundary condition one assumes a constant (independent of x*) longitudinal heat flux where in each cross section the wall temperature is constant independent of y* and z*. This boundary condition may represent, for example, electric resistance heating of highly conductive walls. In case 1 the four walls are uniformly heated and for this case we take the results of [11] for both velocity and temperature profile to investigate the Second Law aspects of the problem. In case 2, one of the walls is assumed to be adiabatic. In case 3, the two sidewalls are assumed to be adiabatic.

To the authors' knowledge, no analytical solution is available for cases 2 and 3 of this problem.

2. ANALYSIS

2.1 Hydrodynamic aspects of the problem

The Darcy-Brinkman extended momentum equation for the case of unidirectional (fully developed) flow in the x^*-direction in a rectangular duct occupied by a porous medium with velocity $u^*(y^*,z^*)$ can be written based on [2]:

$$\tilde{\mu}\left(\frac{\partial^2 u^*}{\partial y^{*2}}+\frac{\partial^2 u^*}{\partial z^{*2}}\right)-\frac{\mu}{K}u^*+G=0\,. \qquad (1)$$

In the above equation, μ is the fluid viscosity, $\tilde{\mu}$ is an effective viscosity, K is the permeability, and G is the negative of the applied pressure gradient. The analytical solution to this equation subject to impermeable wall boundary condition is [11]:

$$\hat{u}=\frac{1}{A}\sum_{n=1}^{\infty}D_n\left(1-\frac{\cosh mz}{\cosh ma}\right)\cos\lambda_n y$$

$$A=\frac{2}{\pi}\sum_{n=1}^{\infty}\frac{1}{(2n-1)^2 m^2}\left(1-\frac{\tanh ma}{ma}\right), \qquad (2\text{-a,b,c})$$

$$D_n=\frac{(-1)^{n-1}}{(2n-1)m^2}\,.$$

where $(x,y,z)=(x^*/Pe,y^*,z^*)/H$ are the dimensionless coordinates, $M=\tilde{\mu}/\mu$ is the viscosity ratio, $Da=K/H^2$ is the Darcy number, $\lambda_n=(2n-1)\pi/2$ are the eigenvalues, $s=(MDa)^{-1/2}$ is the porous media shape parameter, $Pe=\rho c_p U D_H/k$ is the Peclet number, and $m=(s^2+\lambda_n^2)^{1/2}$. Here $\hat{u}$ is the dimensionless velocity defined as

$$\hat{u}=\frac{u^*}{U} \qquad (3)$$

where U is the average velocity defined as $U=\langle u^*\rangle$ (the angle brackets denote an average taken over the duct cross-section).

2.2 Energy-entropy analysis

2.2.1 First Law aspects of the problem

Steady-state condition, local thermal equilibrium, homogeneity, and no thermal dispersion are assumed (one may consult [2] to find the condition based on which one can neglect the

aforementioned effects in the thermal energy equation). In this case the thermal energy equation becomes

$$u^* \frac{\partial T^*}{\partial x^*} = \frac{k}{\rho c_P}\left(\frac{\partial^2 T^*}{\partial y^{*2}} + \frac{\partial^2 T^*}{\partial z^{*2}}\right). \quad (4)$$

Here T^* is the temperature, ρ the density of the fluid, c_P the specific heat at constant pressure of the fluid, and k is the effective thermal conductivity of the medium. The Nusselt number is defined as

$$\mathrm{N}u = \frac{q'' D_H}{k(T_w^* - T_m)}. \quad (5\text{-a})$$

where q'' is the heat transfer rate per unit heat transfer area of the duct (similar to what defined by Shah and London [28]), i.e.

$$q'' = \frac{q'}{P_h}. \quad (5\text{-b})$$

Here, q' is the wall heat transfer rate per unit length of the duct and P_h is the heated perimeter of the duct.

Moreover, the bulk temperature is defined as $T_m = \langle \hat{u} T^* \rangle$ and the hydraulic diameter, D_H, is given by $D_H = 4Ha/(a+1)$.

2.2.2 Second law aspects of the problem

Entropy generation through heat and fluid flow in a porous medium is associated with thermodynamic irreversibility. Different sources are responsible for generation of entropy, including heat transfer across a finite temperature gradient, mixing, and viscous dissipation. Bejan and coworkers [15, 29, 30] focused on the different reasons behind entropy generation in applied thermal engineering systems. Following Bejan [15], the entropy generation rate per unit

volume (called entropy generation hereafter) is related to heat transfer irreversibility due to heat transfer in the direction of finite temperature gradients, HTI, and fluid friction irreversibility due to frictional heating, FFI, as

$$\dot{S}_{gen} = HTI + FFI \tag{6-a}$$

where

$$HTI = k\frac{\left(\frac{\partial T^*}{\partial x^*}\right)^2 + \left(\frac{\partial T^*}{\partial y^*}\right)^2 + \left(\frac{\partial T^*}{\partial z^*}\right)^2}{T^{*2}}, \qquad FFI = \frac{\frac{\mu u^{*2}}{K} + \tilde{\mu}\left(\left(\frac{\partial u^*}{\partial y^*}\right)^2 + \left(\frac{\partial u^*}{\partial z^*}\right)^2\right)}{T^*}. \tag{6-b,c}$$

One notes that in the above equations T^* is measured in Kelvin.

3. SOLUTION PROCEDURE

3.1.1 Case 1

For this case we recover the analytical solution reported in [11] that proposes the following form for the longitudinal temperature gradient

$$\frac{\partial T^*}{\partial x^*} = \frac{q''}{\rho c_P HU}\left(\frac{a+1}{a}\right), \tag{7}$$

The dimensionless temperature profile, $\theta = k\frac{T_w - T^*}{q'' D_H}$, may be rearranged as

$$\theta = \left(\frac{a+1}{2as}\right)^2 \frac{1}{A}\sum_{n=1}^{\infty}\frac{D_n}{\lambda_n^2}\cos\lambda_n y\left(s^2 - m^2\frac{\cosh\lambda_n z}{\cosh\lambda_n a} + \lambda_n^2\frac{\cosh mz}{\cosh ma}\right). \tag{8}$$

The dimensionless form of entropy generation, *Ns*, is defined to be

$$Ns = \frac{\dot{S}_{gen}}{k}\left(\frac{H}{q*}\right)^2, \tag{9}$$

where the dimensionless heat flux, q^*, is

$$q^* = \frac{q'' D_H}{kT_w}. \tag{10}$$

We fixed the q* value to a small one (q*=0.1) through this work so that one can neglect possible changes in the fluid and solid matrix property as a result of high temperature differences in a cross section.

In particular from equations (6-10) one finds *Ns* and *Be* as

$$Ns = \frac{\left(\frac{a+1}{a}\right)^2 + \left(\frac{\partial\theta}{\partial y}\right)^2 + \left(\frac{\partial\theta}{\partial z}\right)^2}{(1-\theta q*)^2} + Br* s^2 \frac{\phi}{(1-\theta q*)},$$

$$Be = \frac{\left(\frac{a+1}{a}\right)^2 + \left(\frac{\partial\theta}{\partial y}\right)^2 + \left(\frac{\partial\theta}{\partial z}\right)^2}{\left(\frac{a+1}{a}\right)^2 + \left(\frac{\partial\theta}{\partial y}\right)^2 + \left(\frac{\partial\theta}{\partial z}\right)^2 + Br* s^2 (1-\theta q*)\phi}. \tag{11-a,b}$$

where the modified Brinkman number, *Br**, is defined as

$$Br* = \frac{\mu U^2}{kT_w q*^2}. \tag{11-c}$$

Moreover, the dimensionless viscous dissipation function, ϕ, is defined as

$$\phi = \hat{u}^2 + s^{-2}\left(\left(\frac{\partial\hat{u}}{\partial y}\right)^2 + \left(\frac{\partial\hat{u}}{\partial z}\right)^2\right). \tag{12}$$

It is worth noting that ϕ remains unchanged while FFI changes from one case to another. All of the terms in equations (11-12) are known and one may find both *Be* and *Ns* by equations (11-a,b). The average values may be found as *Ns**=<*Ns*> and *Be**=<*Be*>. Numerical integration is applied

to find *Ns** and *Be** values since one notes that both *Ns* and *Be* are nonlinear functions of *y* and *z* and analytical solutions are not possible.

3.1.2 Case 2

Here the three walls are kept at a uniform temperature (T_w) while the fourth one (the right wall shown in Fig.1) is adiabatic. For this case the First Law implies that

$$\frac{\partial T^*}{\partial x^*} = \frac{q''}{\rho c_P HU}\left(\frac{2a+1}{2a}\right), \tag{13}$$

Applying the dimensionless temperature profile, the thermal energy equation becomes

$$\frac{\partial^2 \theta}{\partial y^2} + \frac{\partial^2 \theta}{\partial z^2} + \frac{\hat{u}(a+1)(2a+1)}{8a^2} = 0\,. \tag{14}$$

The thermal boundary conditions are $\frac{\partial \theta}{\partial z} = 0$ at the adiabatic wall and $\theta = 0$ at other walls.

The solution satisfying the partial differential equation (14) and the aforementioned boundary conditions may be written as

$$\theta = \sum_{n=1} f_n(z)\cos\lambda_n y\,. \tag{15}$$

After some algebraic manipulation one finds that

$$\theta = \frac{(a+1)(2a+1)}{16 s^2 a^2}\frac{\pi}{A}\sum_{n=1}^{\infty}\frac{(-1)^{n-1}}{\lambda_n^2}\left(A_1\cosh\lambda_n z + A_2\sinh\lambda_n z + \frac{\left(s^2+\lambda_n^2\dfrac{\cosh mz}{\cosh ma}\right)}{\lambda_n m^2}\right)\cos\lambda_n y \tag{16-a}$$

with

$$A_1 = \frac{\lambda_n^2 \tanh 2\lambda_n a\left(\frac{\tanh \lambda_n a}{2\lambda_n} - \frac{\tanh ma}{2m}\right) - 1}{\lambda_n^2 \cosh \lambda_n a}$$
$$A_2 = \frac{\cosh \lambda_n a\left(\frac{\tanh \lambda_n a}{\lambda_n} - \frac{\tanh ma}{m}\right)}{\cosh 2\lambda_n a} \qquad (16\text{-b,c})$$

The compatibility condition (an identity resulting from the definitions)

$$Nu = \frac{1}{\langle \hat{u}\theta \rangle}, \qquad (17)$$

yields an expression for the Nusselt number, namely

$$\mathrm{Nu} = \frac{(2a\pi As)^2}{(2a+1)(a+1)} / \sum_{n=1}^{\infty} \frac{K_n}{(2n-1)^4 m^4}, \qquad (18)$$

where

$$K_n = \frac{\lambda_n^2}{2}\tanh^2 ma - \left(\frac{\lambda_n^2}{2} - s^2\right)\left(1 - \frac{\tanh ma}{ma}\right) + \frac{m^4}{2s^2}\left(\frac{\tanh \lambda_n a}{\lambda_n} - \frac{\tanh ma}{m}\right)$$
$$\left(\lambda_n \tanh 2\lambda_n a\left(\frac{\tanh \lambda_n a}{\lambda_n} - \frac{\tanh ma}{m}\right) - 2\right) \qquad (19)$$

The Second law proposes the following form for *Ns* and *Be*

$$Ns = \frac{\left(\frac{2a+1}{2a}\right)^2 + \left(\frac{\partial\theta}{\partial y}\right)^2 + \left(\frac{\partial\theta}{\partial z}\right)^2}{(1-\theta q^*)^2} + Br^* s^2 \frac{\phi}{(1-\theta q^*)}.$$
$$Be = \frac{\left(\frac{2a+1}{2a}\right)^2 + \left(\frac{\partial\theta}{\partial y}\right)^2 + \left(\frac{\partial\theta}{\partial z}\right)^2}{\left(\frac{2a+1}{2a}\right)^2 + \left(\frac{\partial\theta}{\partial y}\right)^2 + \left(\frac{\partial\theta}{\partial z}\right)^2 + Br^* s^2 (1-\theta q^*)\phi}. \qquad (20\text{-a,b})$$

3.1.3 Case 3

For this case it is assumed that the upper and lower walls are kept at a uniform temperature (T_w) while the sidewalls are adiabatic. The First Law of Thermodynamics implies

$$\frac{\partial T^*}{\partial x^*} = \frac{q''}{\rho c_P H U} . \tag{21}$$

In dimensionless form, the thermal energy equation reads

$$\frac{\partial^2 \theta}{\partial y^2} + \frac{\partial^2 \theta}{\partial z^2} + \frac{\hat{u}(a+1)}{4a} = 0 . \tag{22}$$

The appropriate boundary conditions are $\theta = 0$ at the upper and lower walls and $\frac{\partial \theta}{\partial z} = 0$ at the adiabatic walls (sidewalls). Similar to the previous section one finds the dimensionless temperature distribution as

$$\theta = \frac{a+1}{4aA} \sum_{n=1}^{\infty} \frac{D_n}{\lambda_n^2} \left(1 - \frac{\lambda_n m \tanh ma}{s^2} \frac{\cosh \lambda_n z}{\sinh \lambda_n a} + \frac{\lambda_n^2}{s^2} \frac{\cosh mz}{\cosh ma} \right) \cos \lambda_n y , \tag{23}$$

and consequently one finds the Nusselt number as

$$\mathrm{Nu} = \frac{2(\pi As)^2 a}{(a+1)} \Big/ \sum_{n=1}^{\infty} \frac{F_n}{(2n-1)^4 m^4} , \tag{24}$$

where

$$F_n = \left(\frac{\lambda_n^2}{2} - s^2 \right) \left(1 - \frac{\tanh ma}{ma} \right) - \frac{m^4}{s^2} \frac{\tanh ma}{m} \left(1 - \frac{\lambda_n}{m} \frac{\tanh ma}{\tanh \lambda_n a} \right) + \frac{\lambda_n^2}{2} \tanh^2 ma . \tag{25}$$

Similar to the previous section, *Ns* and *Be* are found to be

$$Ns = \frac{1+\left(\frac{\partial\theta}{\partial y}\right)^2+\left(\frac{\partial\theta}{\partial z}\right)^2}{(1-\theta q^*)^2} + Br^* s^2 \frac{\phi}{(1-\theta q^*)},$$

$$Be = \frac{1+\left(\frac{\partial\theta}{\partial y}\right)^2+\left(\frac{\partial\theta}{\partial z}\right)^2}{1+\left(\frac{\partial\theta}{\partial y}\right)^2+\left(\frac{\partial\theta}{\partial z}\right)^2 + Br^* s^2 (1-\theta q^*)\phi}. \qquad (26\text{-a,b})$$

4. RESULTS AND DISCUSSION

Closed form solutions have been obtained for the variation of velocity, temperature, the Bejan number, and the dimensionless entropy generation function throughout the solution domain. In the interest of brevity, we will limit our results to the effect of the duct aspect ratio and shape parameter on Nu, *Be*, and *Ns*.

Figure 2 shows the Nusselt number for all the three cases studied versus the shape parameter. As a common trend, *Nu* seems to increase with the aspect ratio, *a*. One should, however, note that this trend is primarily due to the choice of the length scale in the definition of *Nu*. If the Nusselt number were based on 4*H*, for example, instead of the hydraulic diameter, D_H, the dependence on the aspect ratio would almost completely disappear. This shows the importance of recognizing the way the dimensionless parameters are constructed when interpreting the physical implications of graphs such as Figure 2. The values at the low end of the *s* axis are expected to converge to the clear fluid conditions. In fact, they do so below *s*=1 and show very good agreement against values reported in literature for heat transfer in rectangular ducts with clear fluids, e.g. [28]. It is interesting to note that Shah and London [28] also based the Nusselt number on the hydraulic diameter, which emphasizes the dependence on the aspect ratio as mentioned above. The values at the high end of the *s* axis should approach the Darcy flow

conditions. In fact, the Nusselt number seem to attain its Darcy flow value at around s=50-70 regardless of neither the aspect ratio nor the boundary conditions. For s values approximately between 1 and 70, Nu shows a power relation with s, increasing from its clear fluid value to almost its slug flow limit over this range. When examining the differences due to the heat transfer boundary conditions, one should remember that the heat flux in the Nusselt number definition (Eqs 5a and 5b) is based on the heated perimeter rather than the wetted perimeter. This follows the general practice to facilitate comparison against past results reported in the literature [28]. It appears that the case 1 boundary condition almost always results in the lowest Nusselt number at the clear fluid end (as s approaches 0) of all three boundary condition cases. The only exception is for the square duct (a=1), where Nu_2 values are consistently below the other two cases over entire *s* domain, but even there the clear fluid values for cases 1 and 2 are very close to each other. In general, for small *s* values Nu_3 is higher than Nu_1 while for higher *s* values it is the other way around. For clear fluid or hyperporous flow through square ducts, case 3 results in a higher Nu value with the same pressure drop. As s increases for a square duct, e.g. keeping a fixed duct size when the permeability is lowered, case 1 provides the highest Nusselt number. In addition to having a higher Nusselt number over the heat transfer area, it should be remembered that the actual heat transfer area is also higher for the case 1 boundary condition. Therefore, flow through a square duct with low permeability achieves the best heat removal rates under case 1 boundary conditions. This fact may be of vital importance when it comes to applications such as low permeability foam for cooling electronic equipment similar to the Al-foam examined by Lage et al. [31]. However, with rectangular cross sections, the situation starts changing in such a way that Nu_1 goes to minimum regardless of the *s* value. Considering rectangular porous passages with small *s* values, Nu_3 is always higher than the other two. On the other hand for

higher *s* values approaching slug flow conditions, Nu2 exceeds Nu3 (and Nu1 non-square ducts). This does not change the fact that if one needs to achieve maximum cooling rate, all four surfaces must be used. However, our results show that there is some compensation offered by higher Nusselt numbers over smaller heat transfer areas if one has to limit the heat exchange area for other reasons.

Another point worth mentioning is that for very large aspect ratios all of the three cases resemble parallel plate channel case where the *Nu* plots become almost indistinguishable. This is expected since for very large values of *a*, heat transfer rate from the two short sidewalls is negligible compared to the total heat transfer rate.

To explain the Nu behavior, we classify the results in terms of high ($s>>10$) and low porous media shape parameters ($s<<10$). For small s values, case 3 achieves the highest Nusselt number values. This case has two adiabatic walls near which the temperature shows no change in the direction normal to the walls. This means that in this region the heat transfer is almost one dimensional (along the side walls) and the temperature is not equal to T_w. This means that the minimum temperature, which is expected to happen in the duct center for being in its farthest distance from the walls, is higher than the minimum value for the other two cases when the heat input to the duct as our thermodynamic system (which will change the enthalpy of the system) is constant for the three cases. Considering the fact that in the duct center the velocity experiences its maximum, one expects that the bulk-wall temperature difference (which is inversely proportional to Nu) be minimum compared to the other counterparts leading to an increase in Nu. However, when *s* increases to higher values, say $s>10$, the situation changes in such a way that the velocity changes are restricted to thin near wall regions [11] and out of this region the velocity distribution is uniform. For large *s* values there are two opposing effects: near the

adiabatic walls the heat transfer is one dimensional and this enhances the minimum temperature at the duct center compared to a case with no adiabatic wall, i.e. case 1. On the other hand, high near wall temperatures when one has heated walls are associated with small velocity values due to wall effects. Case 2 acts somewhere between the two others in such a way that near the adiabatic wall isotherms of case 2 are similar to that of case 3 but near the heated wall they resemble case 1. It seems that for this reason case 2 leads to higher Nu values for rectangular cross sections when the porous media shape parameter is large. When it comes to a square cross section, case 1 delivers the highest Nusselt number and this is justified when one observes that the diagonal lines are adiabatic lines along which no heat is transferred and isotherms are normal to these lines, similar to a pure conduction problem. This will lead to a circle-like temperature distribution which is more uniform compared to the other cases since, to a good extent, the duct cross section can be considered as a sum of 8 similar triangles each of which formed by two adiabatic lines and half of a wall. In a nutshell, the center-wall temperature difference is smaller than the other cases with a net effect of decreasing wall-bulk temperature difference and increasing Nu. However, with rectangular cross sections the diagonal symmetry will no more exist for case 1.

Figures 3-a and 3-b show Ns^* versus a for s=1 and s=10, respectively. A quick check of the both figures shows that the dimensionless average entropy generation rate appears to be decreasing with an increase in the duct aspect ratio regardless of the s value. As it was already noted for the Nusselt number above, the choice of the length scale must be recognized in interpreting these results. To facilitate comparisons with past literature, the non-dimensional entropy generation is based on the hydraulic diameter as shown in Eqs. 9 and 10. The dimensionless entropy generation is higher for the square cross section compared to the

rectangular counterparts and this is similar to what reported by previous researchers [17], [32]. Moreover, comparing the *Ns** levels in the two figures one realizes that increasing *s* increases *Ns**. Another feature of considerable interest is that, regardless of *s* and *a* value, case 1 is the most irreversible design while case 3 produces the least entropy. In the view of the above, one concludes that the least effective design is that of case 1 with a=1 and s=10. For this reason we gave this case a special attention within the rest of our study.

Figures 4-a,b show the line diagrams of *Be* and *Ns* for a better understanding of the problem. Figure 4-a illustrates *Be* versus *y* at four *z* locations. One observes that *Be* is more or less constant excluding a thin near wall region where for *z*=0.9, *Be* reaches its maximum value while at smaller *z* the Bejan number increases and then decreases to its minimum value at the wall. It is also clear that in this case, *Be* is less than 0.5 and hence FFI>HTI. This was expected since in this case *s* is large enough for FFI to become comparable with HTI.

Comparing figure 4-b with the previous one, one observes that *Ns* plots are in opposite direction to those of *Be* in such a way that the maximums/minimums of *Ns* are associated with the minimums/maximums of *Be*. With z=0.9 the value of *Ns* increases from wall to the duct center while at other *z* locations *Ns* decreases from the wall to a near-wall minimum, increases and then remains constant up to the duct center. According to this figure, the walls are the most active entropy generation sites where both of the temperature and velocity gradients experience their maximum values and consequently both HTI and FFI increase with the net effect of increasing *Ns*. One notes that *Ns* value at the duct center is not a minimum one. This fact is unique for a porous passage and in the clear fluid case one expects *Ns* to be minimum since both velocity and temperature gradients vanish due to symmetry. A quick check of the *Ns* function shows that moving from the walls to the channel center, the Darcy dissipation term (which is

absent in the clear fluid case) will grow since the boundary effects will not be felt and FFI, which is proportional to u^2, will never vanish. One can consult Nield [33] for a recent note of viscous dissipation in a porous medium.

5. CONCLUSION

Analytical solutions are reported for the temperature distribution and the Nusselt number that cover three different boundary conditions. It is found that, for $s<10$, the best use of the heat transfer area in view of the best heat transfer rate (with the same pressure drop) is achieved by case 3. However, for $s>10$ the optimum design is dependent on a value in such a way that for a duct of square cross-section, case 1 acts better than the others while for other values of a, case 2 provides the best heat transfer rate. Having known the velocity and temperature profile, the Second Law analysis of the problem is presented. It is found that case 3 is the best design for having the minimal lost work, with the same a and s values, while case 1 is associated with the highest entropy production value among the others.

Acknowledgments

The first author, the scholarship holder, acknowledges the support provided by The University of Queensland in terms of UQILAS, Endeavor IPRS, and School Scholarship. Ali A. Merrikh acknowledges the support provided by the *Thermal Center of Excellence* of Applied Thermal Technologies, LLC (www.thermalcooling.com).

References

[1] A. Narasimhan, J. L. Lage, Modified Hazen-Dupuit-Darcy model for forced convection of a fluid with temperature-dependent viscosity, ASME J. Heat Transfer 123 (2001) 31-38.

[2] D.A. Nield, A. Bejan, Convection in Porous Media, 3rd ed, Springer-Verlag, New York, 2006.

[3] P. Cheng, Heat Transfer in Geothermal Systems, Adv. Heat Transfer 14 (1978) 1-105.

[4] A. Haji-Sheikh, K. Vafai, Analysis of flow and heat transfer in porous media imbedded inside various-shaped ducts, Int. J. Heat Mass Transfer 47 **(**2004) 1889-1905.

[5] A. Haji-Sheikh, Fully developed heat transfer to fluid flow in rectangular passages with filled with porous materials, ASME J. Heat Transfer 128 (2006) 822–828.

[6] A. Haji-Sheikh, W. J. Minkowycz, E. M. Sparrow, Green's function solution of temperature field for flow in porous passages, Int. J. Heat Mass Transfer 47 (2004) 4685-4695.

[7] A. Haji-Sheikh, D. A. Nield, K. Hooman, Heat transfer in thermal entrance region for flow through rectangular porous passages, Int. J. Heat Mass Transfer 49 (2006) 3004–3015

[8] A. Haji-Sheikh, W. J. Minkowycz, E. M. Sparrow, A numerical study of the heat transfer to fluid flow through circular porous passages, Num. Heat Transfer A 46 (2004) 929-955.

[9] A. Haji-Sheikh, E. M. Sparrow, W. J. Minkowycz, Heat transfer to flow through porous passages using extended weighted residuals method–A Green's function solution, Int. J. Heat Mass Transfer 48 (2005) 1330-1349.

[10] A. Haji-Sheikh, Estimation of average and local heat transfer in parallel plates and circular ducts filled with porous materials, ASME J. Heat Transfer 126 (2004) 400–409.

[11] K. Hooman, A. A. Merrikh, Analytical solution of forced convection in a duct of rectangular cross-section saturated by a porous medium, ASME J. Heat Transfer 128 (2006) 596-600.

[12] K. Hooman, Fully developed temperature distribution in a porous saturated duct of elliptical cross-section, with viscous dissipation effects and entropy generation analysis, Heat Transfer Research 36 (2005) 237-245.

[13] K. Hooman, Analysis of entropy generation in porous media imbedded inside elliptical passages, Int. J. Heat Technology 23 (2005) 145-149.

[14] K. Hooman, H. Gurgenci, Effects of temperature-dependent viscosity variation on entropy generation, heat, and fluid flow through a porous-saturated duct of rectangular cross-section, submitted to Appl. Math. Mech.

[15] A. Bejan, Entropy Generation through Heat and Fluid Flow, Wiley, New York, 1982.

[16] I. Dagtekin, H. F. Oztop, A. Z., Sahin, An analysis of entropy generation through a circular duct with different shaped longitudinal fins for laminar flow, Int. J. Heat Mass Transfer 48 (2005) 171-181.

[17] Ratts E.B., Raut A.G., Entropy generation minimization of fully developed internal flow with constant heat flux, ASME J. Heat Transfer 126 (2004) 656-659.

[18] A.C. Baytas, Entropy generation for natural convection in an inclined porous cavity, Int. J. Heat Mass Transfer 43 (2000) 2089-2099.

[19] A.C. Baytas, Entropy generation for free and forced convection in a porous cavity and a porous channel, in Emerging Technology and Techniques in Porous Media (Eds. D.B. Ingham et al.), Kluwer Academic Publishers (2004) 259-270.

[20] D.A. Nield, Resolution of a paradox involving viscous dissipation and nonlinear drag in a porous medium, Transport Porous Media 41 (2000) 349-357.

[21] A.K. Al-Hadrami, L. Elliott, D.B. Ingham, A new model for viscous dissipation in porous media across a range of permeability values, Transport Porous Media 53 (2003)117-122.

[22] D.A. Nield, A.V. Kuznetsov, M. Xiong, Effects of viscous dissipation and flow work on forced convection in a channel filled by a saturated porous medium, Transport Porous Media 56 (2004) 351-367.

[23] K. Hooman, H. Gurgenci, Effects of viscous dissipation and boundary conditions on forced convection in a channel occupied by a saturated porous medium, submitted to Transport Porous Media

[24] K. Hooman, A. Pourshaghaghy, A. Ejlali, Effects of viscous dissipation on thermally developing forced convection in a porous saturated circular tube with an isoflux wall, Appl. Math. Mech. 27 (2006) 617-626.

[25] D.A. Nield, Comments on 'A new model for viscous dissipation in porous media across a range of permeability values' by A. K. Al-Hadrhrami, L. Elliott and D. B. Ingham, Transport Porous Media 55 (2004) 253-254.

[26] K. Hooman, A. Ejlali, Second law analysis of laminar flow in a channel filled with saturated porous media: a numerical solution, Entropy 7 (2005) 300-307.

[27] K. Hooman, A. A. Merrikh, A. Ejlali, Comments on "Flow, thermal, and entropy generation characteristics inside a porous channel with viscous dissipation" by S. Mahmud and R.A. Fraser, Int. J. Thermal Sciences, in press.

[28] R. K. Shah, A. L. London, Laminar Flow Forced Convection in Ducts (Advances in Heat Transfer, Supplement 1), Academic Press, New York, 1978.

[29] A. Bejan, I. Dincer, S. Lorente, A. F., Miguel, A. H., Reis, Porous and Complex Flow Structures in Modern Technology, Springer-Verlag, New York, 2004.

[30] A. Bejan, Advanced Engineering Thermodynamics, 2nd Ed., Wiley, New York, 1997.

[31] J. L. Lage, B. V. Antohe, D. A. Nield, Two types of nonlinear pressure-drop versus flow rate observed for saturated porous media, ASME J. Fluids Engng. 119 (1997) 700-706.

[32] A. Z. Sahin, Irreversibilities in various duct geometries with constant wall heat flux and laminar flow, Energy 23 (1998) 465–473.

[33] D. A. Nield, A note on a Brinkman-Brinkman forced convection problem, Transport Porous Media 64 (2006) 185-188.

Table 1 Case definition in terms of the boundary conditions

Case	Entity name	Boundary condition
1	AB, BC, CD, DA	Heated
2	CD	Insulated
	AB,BC, DA	Heated
3	BC, AD	Heated
	AB, CD	Insulated

Figure Captions

Figure 1 Definition sketch

Figure 2 The Nusselt number versus the porous media shape parameter for the three cases with some aspect ratios

Fig 3 Average dimensionless entropy generation for the three cases versus the aspect ratio, (A) s=1 and (B) s=10

Fig 4 (A) Local Bejan number and (B) local dimensionless entropy generation for case 1 with s=10 for a duct of square cross section

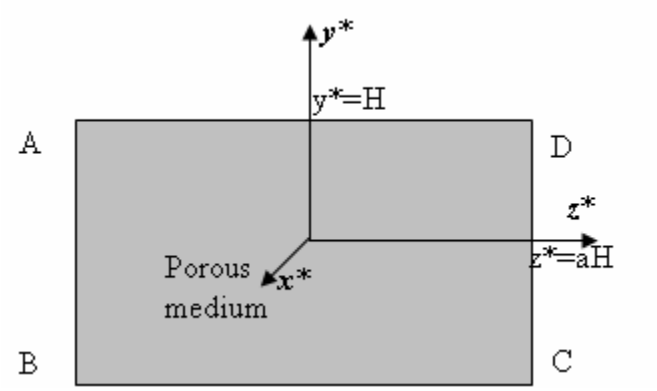

Figure 1 Definition sketch

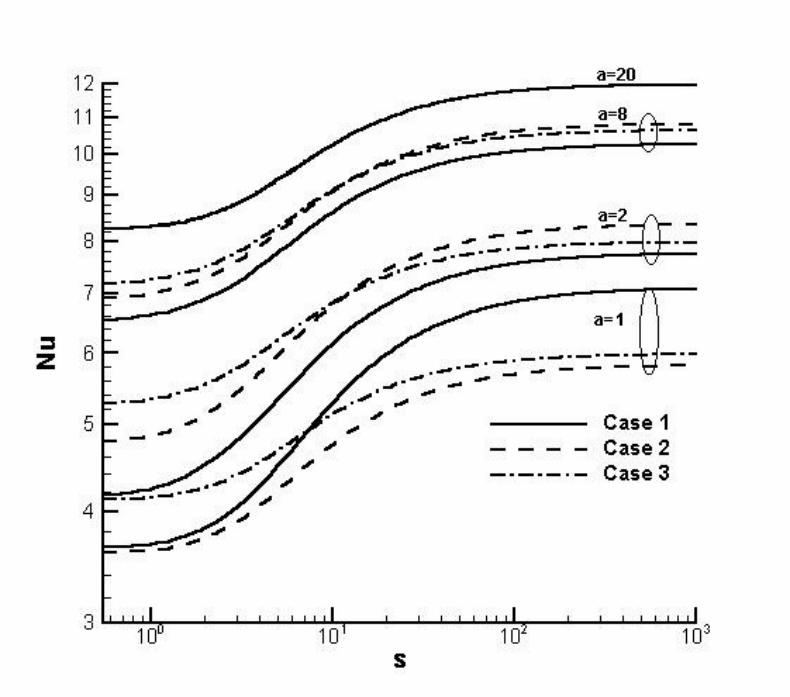

Figure 2 The Nusselt number versus the porous media shape parameter for the three cases with some aspect ratios.

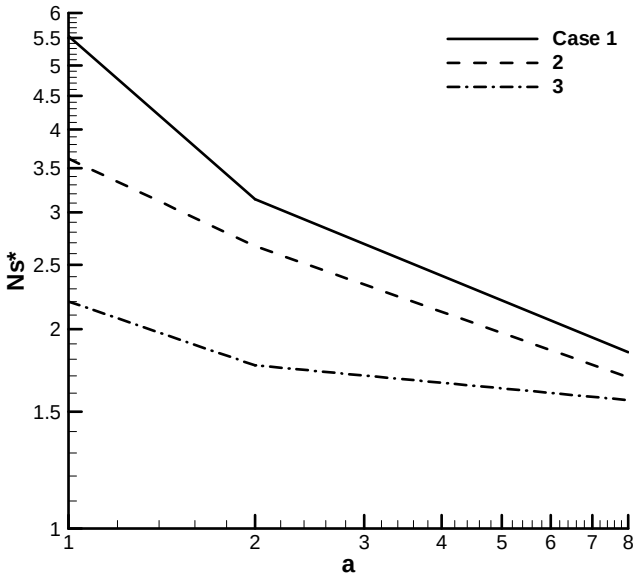

3-A

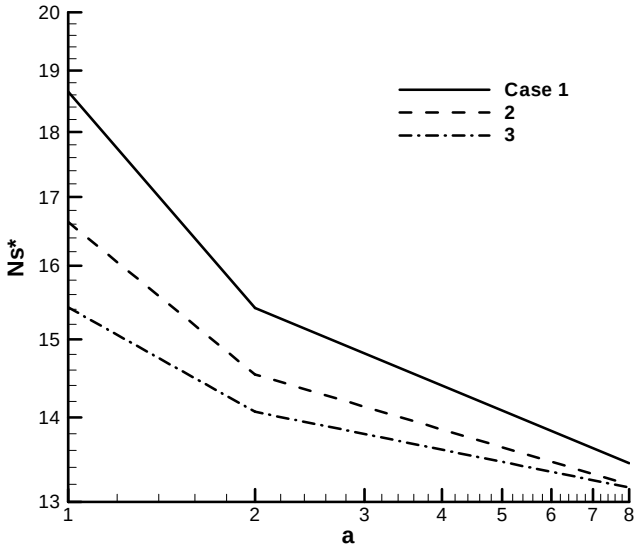

3-B

Fig 3 Average dimensionless entropy generation for the three cases versus the aspect ratio, (A) s=1 and (B) s=10

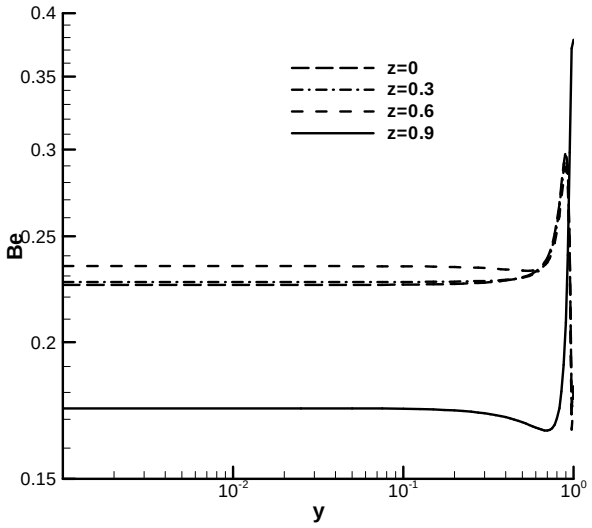

4-A

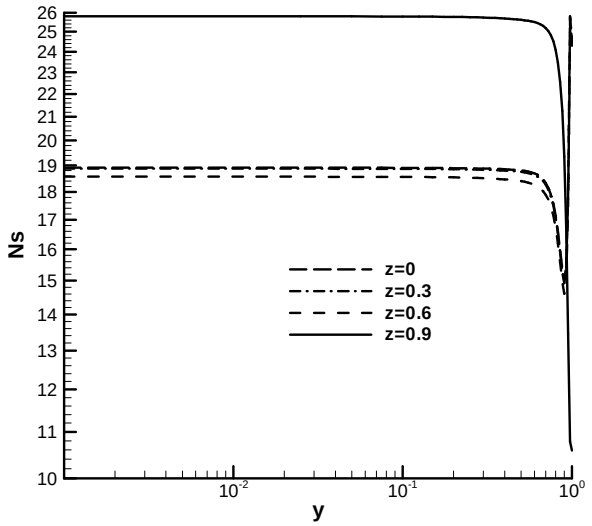

4-B

Fig 4 (A) Local Bejan number and (B)local dimensionless entropy generation for case 1 with s=10 for a duct of square cross section